Construction and Building Materials 220 (2019) 43–52

Contents lists available at ScienceDirect

Construction and Building Materials

journal homepage: www.elsevier.com/locate/conbuildmat

Chloride immobilization of cement-based material containing nano-Al_2O_3

Xiaohai Liu [a], Baoguo Ma [a], Hongbo Tan [a,*], Hainan Li [b,*], Junpeng Mei [a], Ting Zhang [a], Pian Chen [a], Benqing Gu [c]

[a] State Key Laboratory of Silicate Materials for Architectures, Wuhan University of Technology, Wuhan 430070, China
[b] Department of Construction Cost, Wuhan Textile University, Wuhan 430200, China
[c] First Department of New Materials, Guangzhou Institute of Building Science, Guangzhou 510440, China

HIGHLIGHTS

- Chloride immobilization can be improved by adding NA into cement.
- NA strengthens chemical binding by increasing the content of chloroaluminates.
- NA improves migration resistance by refining the pore structures.

ARTICLE INFO

Article history:
Received 25 February 2019
Received in revised form 22 April 2019
Accepted 24 May 2019
Available online 6 June 2019

Keywords:
Internal chloride
Rebar corrosion
Cement-based materials
Nano-Al_2O_3

ABSTRACT

The utilization of marine resources in reinforced concrete is severely limited, due to the risk of steel corrosion caused by the introduced chloride. In order to reduce this risk, nano-Al_2O_3 (NA) was added into cement-based materials system by improving the chloride immobilization. The immobilized chloride ratio (ICR) of the system was evaluated, and the results indicated that the addition of NA could significantly enhance ICR. Based on the results from TG, XRD, ^{27}Al NMR, MIP, ^{29}Si NMR, and EDS, the mechanism behind was discussed from three aspects of chemical binding, migration resistance, and physical adsorption. The reasons for the increased ICR were as follows: a) chemical binding was promoted by increasing the amount of chloroaluminates; b) migration resistance was improved by refining the pore structure; c) physical adsorption, depending on the amount and the Ca/Si ratio of C-S-H gel, was reduced negligibly. These findings can provide guidance for the theoretical study of chloride immobilization and the application of marine resources.

1. Introduction

The utilization of marine resources, such as sea sand and coral sand, has great potential in marine concrete engineering, especially in reef construction in the distant sea. However, the direct use of these resources has been banned in reinforced concrete, due to the potential risk of steel bar corrosion induced by the diffused chloride ions. In order to resist this risk, corrosion inhibitors are usually used in concrete to produce a protective film on the surface of rebar [1–3]. However, due to the existence of large amounts of internal free chloride ions, the risk of pitting corrosion is not completely eliminated by inhibitors. In this case, the chloride immobilization is considered to be another promising way [4,5].

The mechanism of chloride immobilization can be divided into three aspects: chemical binding, physical adsorption, and migration resistance [6,7]. Chemical binding is related to the chloride ions bound in Friedel's salt (FS) or Kuzel's salt (KS). Physical adsorption mainly depends on chloride adsorption by electrical double layers on the surface of calcium-silicate-hydrate (C-S-H) gel [8,9]. Migration resistance is another physical way to hinder the transport of chloride ion, by refining the pore structure to block the channel [10].

The chloride immobilization capacity of cementitious materials could be improved by using supplementary cementitious materials (SCM), including fly ash, ground granulated blast furnace slag, and metakaolin [11–15]. One explanation was confirmed that the increase of the amount of chloroaluminates (i.e., FS and KS) enhanced the chemical binding of chloride ion, which was facilitated by the pozzolanic reaction of SCM rich in aluminum [16–18]. Nanoparticles, such as nano-TiO_2 and nano-$CaCO_3$, were also

* Corresponding authors.
E-mail addresses: thbwhut@whut.edu.cn (H. Tan), 2016007@wtu.edu.cn (H. Li).

https://doi.org/10.1016/j.conbuildmat.2019.05.148
0950-0618/

used to resist the penetration of chloride ions to extend durability [19,20].

However, a seven-year-long observation have found that the chloride immobilization of the cement-based materials decreased with the extension of the curing age, resulting in high corrosion risk [21]. Due to the fact that the chemical binding is a large part of chloride ion immobilization [17], this result might be attributed to the reduction in chemical binding. And according to the literatures, the stability of chloroaluminates is influenced by factors such as alkalinity, active aluminum content, and Al/Si ratio of C-S-H gel. In cement-silica fume system, the pozzolanic reaction of silica fume reduced the alkalinity value, resulting in poor stability of chloroaluminates, explained by Eqs. (1) and (2) [22,23]. Andrej Ipavec et al. reported that the presence of alkalis hindered the formation of chloroaluminates at low chloride concentrations [24]. Thomas et al. found that the binding capacity of fly ash was not related to the total alumina content, but to the active aluminum content [25]. And studies revealed that part of active aluminum could replace Si in C-S-H gel to form C-A-S-H gel, which decreased the effective aluminum content for keeping the stability of chloroaluminates [26]. Based on these researches, a hypothesis is proposed that continuous and slow supply of active aluminum phase in the system could improve the stability of chloroaluminates and even increase the amount of these salts.

$$\left[Ca_2Al(OH)_6 \cdot 2H_2O\right]_2 \cdot Cl_2 \cdot 4H_2O \rightleftharpoons 4Ca^{2+} + 2Al(OH)_4^- + 4OH^- + 2Cl^- + 8H_2O \quad (1)$$

$$\left[Ca_2Al(OH)_6 \cdot 2H_2O\right]_2 \cdot (SO_4)_{0.5} \cdot Cl \cdot 6H_2O \rightleftharpoons 4Ca^{2+} + 2Al(OH)_4^- + 4OH^- + Cl^- + 0.5\,SO_4^{2-} + 10H_2O \quad (2)$$

The nano-Al_2O_3 (NA) has moderate reaction activity during the cement hydration. In the early stage, it mainly exerted filling effect; and with time going on, the aluminum phase of NA could be slowly and continuously released by the pozzolanic reaction [27–30]. In this case, two advantages of NA are expected in chloride immobilization: a) compared with the traditional SCM, NA as a nano-scale material can effectively refine the pore structure to resist the transportation of chloride ion; b) in comparison with other nano-materials, NA rich in aluminum is beneficial to the formation of chloroaluminates.

In this paper, effects of nano-Al_2O_3 on the chloride immobilization were investigated from three aspects: chemical binding, migration resistance, and physical adsorption. The chemical binding dependent on contents of FS and KS was evaluated based on thermo-gravimetric analysis (TGA), X-ray diffraction (XRD), and ^{27}Al nuclear magnetic resonance (^{27}Al NMR). The migration resistance related to the pore structure was characterized by mercury intrusion porosity (MIP). The physical adsorption was analyzed in two aspects: the amount of C-S-H gel evaluated by ^{29}Si nuclear magnetic resonance (^{29}Si NMR), and the Ca/Si ratio of C-S-H gel verified by Energy Disperse Spectroscopy (EDS). Finally, the distribution of chloride ion in cement-based materials could be revealed, and the mechanism behind was discussed. These findings could provide guidance for the theoretical study of chloride immobilization and the application of marine resources.

2. Experimental

2.1. Materials

Type I Portland cement used in this experiment was composed of clinker and gypsum in accordance with requirements of GB 8076-2008 (Chinese standard). The chemical composition of cement obtained from X-ray Fluorescence (XRF, Axios advanced, made by PA Nalytical B.V., Holland) is presented in Table 1.

The commercial NA powder was supplied by Aladdin Industrial Corporation in China. The XRD pattern of NA is presented in Fig. 1, where the broad peaks suggest the amorphous structure. The diffraction peaks of $2\theta = 37.59°$, 39.88°, 46.06°, 61.01°, and 67.14°, can be observed, which confirms the γ crystal form of alumina [29]. The information from the supplier indicated purity of 99.99% and an average particle size less than 20 nm.

2.2. Sample preparation

The cement-based material pastes were prepared with the water/binder ratio of 0.4. Chloride ions were introduced by adding NaCl. And NA was added as a binder, replacing cement with the ratio of 0.25%, 0.5%, 1%, 2%, and 4%. A commercially available polycarboxylate superplasticizer (PCE) was used to adjust the fluidity of paste. Paste formulas are listed in Table 2.

The solution composed of Na, NaCl and deionized water was dispersed by ultrasonic wave. Then this solution was mixed with the cement. And the workability of the paste was controlled by addition of PCE, tested with mini slump (170 ± 10 mm) following the Chinese standard GB/T 8077-2012. Thereafter, the paste was cast in 40 mm × 40 mm × 40 mm cubic moulds. After a curing in chamber with ≥95% R.H. and 20 ± 2 °C for one day, the hardened paste was demoulded. Then the paste was cured in a 20 ± 2 °C temperature, and wrapped with plastic film, to isolate the vapor and carbon dioxide in the air. At the age of 28 d, 90 d, and 180 d, samples were crushed, and the pieces were immersed in ethanol for 5 days to stop hydration. After that, these pieces were dried in a vacuum at 40 °C for 6 h. Some pieces were prepared for EDS and MIP, and the other pieces were grinded into powders. Powders which could pass through a sieve of 0.15 mm, were used in the measurement of chloride immobilization capacity. And the powders with particle size less than 45 μm were prepared for analysis of hydration products (XRD, TGA, and NMR).

2.3. Methods

2.3.1. Immobilized chloride ratio (ICR)

ICR refers to the ratio of the content of immobilized chloride (C_b) and the content of total chloride (C_t). C_b was the difference between C_t and the content of residual free chloride (C_f) [31]. C_t was calculated out according to the content of chloride ions added into the fresh cement paste listed in the formula. Further, corrected by the lost 25% free water during the ethanol immersion and drying, the calculated C_t in the dried hardened cement paste is 5.405 mg chloride ion/g binder.

The value of C_f was determined through leaching and titration method, complying with the Chinese standard of Test Code for Hydraulic Concrete (SL 352-2006). 10.00 g hardened cement paste powder cured for required age was immersed into 100 mL deion-

Table 1
Chemical composition (wt%) of cement.

Composition	SiO_2	CaO	MgO	Fe_2O_3	Al_2O_3	SO_3	Na_2O	K_2O	Ignition loss
Cement	20.06	63.32	2.46	3.02	5.28	2.69	0.06	0.76	1.81

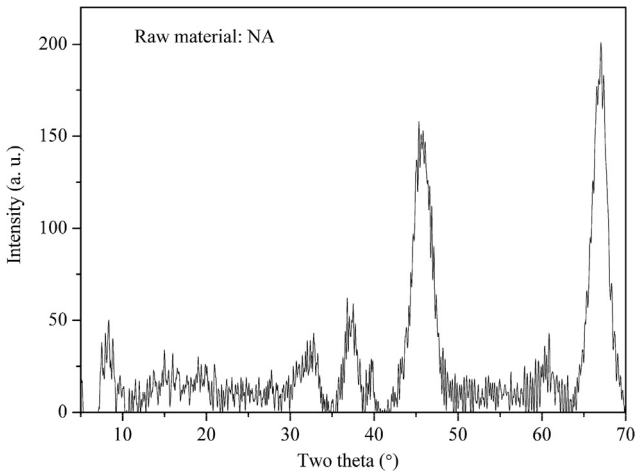

Fig. 1. The XRD pattern of NA.

Table 2
Mix proportion (wt%) of paste.

Sample	Cement	NA	Deionized water	NaCl
CNA0	100	0	40	1.17
CNA0.25	99.75	0.25	40	1.17
CNA0.5	99.5	0.5	40	1.17
CNA1	99	1	40	1.17
CNA2	98	2	40	1.17
CNA4	96	4	40	1.17

ized water. Then the suspension was shocked for 1–2 min and stored for 24 h. Thereafter, the filtrate was obtained by filtration, and the chloride concentration was titrated according to Mohr method. Finally, C_f was calculated out based on the titration results. Each titration was conducted twice, and the average was taken as the final result.

2.3.2. TGA

The phase assemblage was verified by TGA, conducted with the comprehensive thermal analyzer (STA449F3, made by NETZSCH, Germany). The specimen was heated at a rate of 10 °C/min from the room temperature to 1000 °C in N_2 atmosphere. According to the characteristic weight loss peak in DTG pattern, the content of calcium hydroxide (CH) could be gained from TG data.

2.3.3. XRD/RIR

The phase assemblage was also characterized by X-ray diffractometer (XRD, D/Max-RB) with Cu (Kα) radiation and a current of 40 mA and 40 kV. And the test rate was 2°/min with a step of 0.02°.

Reference intensity ratio (RIR) relates to a method to conduct semi-quantitative analysis on the relative mass ratio based on the XRD data. In this experiment, XRD/RIR analysis could indicate the relative mass ratios of CH to FS and CH to KS [32]. Since the CH content was obtained in TGA, contents of FS and KS could be calculated out respectively.

2.3.4. ^{27}Al MAS NMR spectroscopy

^{27}Al MAS NMR spectroscopy was conducted in this experiment, using a Bruker Advance III400 spectrometer. Operating parameters included 10 kHz rotation frequency, 2 s delay time, and the solution of $Al(NO_3)_3{\cdot}9H_2O$ as a standard for ^{27}Al.

In terms of the detection of aluminum-containing phase, XRD characterized only the phase with crystalline structure, while ^{27}Al MAS NMR could well detect aluminates with various local structures, including amorphous and crystalline phases. Thus, ^{27}Al MAS NMR spectroscopy is a valuable analytical tool for investigating the distribution of aluminum, referring to aluminum coordinated in different forms, including tetrahedrons, octahedrons, etc. Furthermore, the spectrum was processed with commercial solid-state NMR software package, including adjusting the phase, correcting baseline and iterative fitting. And the peak shapes were constrained with Gaussian function.

2.3.5. MIP

Since the addition of NA into the cement-based materials notably affected the pore structure, MIP was conducted to characterize this effect on pore size distribution. The mercury intrusion porosimetry (Poremaster GT-60, Kangta Instrument Company, USA) was operated at a maximum pressure of 420 MPa with the contact angle of 140°. And the tested sample was prepared with 3–5 mm dried hardened cement pieces.

2.3.6. ^{29}Si MAS NMR spectroscopy

^{29}Si MAS NMR (solid-state nuclear magnetic resonance) spectroscopy was conducted in this experiment, using a Bruker Advance III400 spectrometer. Operating parameters included 5 kHz rotation frequency, 5 s delay time, and tetramethylsilane as a standard for ^{29}Si.

In NMR spectrum of hydrated cement-NA paste, four peaks were seen clearly: Q^0, Q^1, Q^2 and $Q^2(1Al)$, presenting Si-O tetrahedrons in different chemical states [33,34]. After the processing of spectrum including baseline correction and fitting, the main chain length (MCL) of C-S-H gel and the ratio of Si in C-S-H gel chain substituted by Al (Al/Si) were calculated as follows:

$$MCL = \frac{2I\left(Q^1\right)+2I\left(Q^2\right)+3I[Q^2(1Al)]}{I(Q^1)} \quad (3)$$

$$Al/Si = \frac{0.5I[Q^2(1Al)]}{I\left(Q^1\right)+I\left(Q^2\right)+I[Q^2(1Al)]} \quad (4)$$

The hydration degree of cement (A_C) could also be evaluated as Eq. (5):

$$A_C(\%) = 1\text{-}\frac{I(Q^0)}{I_0(Q^0)} \quad (5)$$

Wherein, $I(Q^n)$ was the integrated intensities of signals of Q^n in hydrated sample; $I_0(Q^n)$ was the integrated intensities of signals of Q^n in unhydrated cement mixture.

2.3.7. EDS

In this work, EDS was used to evaluate the Ca/Si ratio of the C-S-H gel. And the tested sample was prepared from the hardened cement pieces, followed by being dried under vacuum, polished and platinum-coated. An energy dispersive spectrometer, provided by EDAX Inc., USA, was used with an acceleration voltage of 20 keV and a working distance of 10 mm. EDS reports were given by TEAM™ software (supplied by EDAX Inc., USA). The test points for EDS dot scanning were chosen in the zone of C-S-H gel, and the final Ca/Si ratio was the average of numerous points.

2.3.8. Thermodynamic modeling

Thermodynamic modeling was conducted with the Gibbs free energy minimization software (GEMS), and the relevant cement data was supplied by PSI-GEMS database [35]. Based on the thermodynamic calculation aiming to minimize the Gibbs free energy of the system, the equilibrium phase assemblage was obtained for a given total bulk elemental composition.

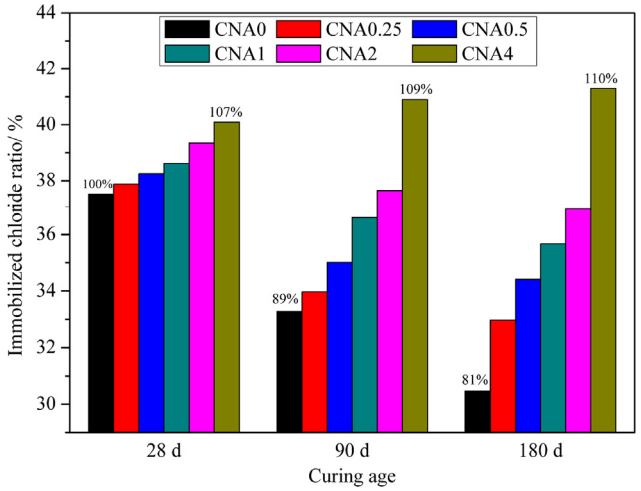

Fig. 2. ICRs of samples with different NA dosages (0–4%) at the age of 28 d, 90 d, and 180 d.

In this experiment, the addition of alumina up to 4% expanded the content of aluminum in the cement paste, and significantly changed the final phase assemblage. Although some defects existed in this modeling (for instance, the adsorption of aluminum by C-S-H gel was not considered), the given result could still provide important guidance.

3. Results and discussion

3.1. Chloride immobilization capacity

In Fig. 2, the results of chloride immobilization capacity are presented. The ICR of the reference sample (CNA0) at 28 d is defined as 100%, and the relative ratios of ICR of other samples is also labeled.

As shown in Fig. 2, at the same curing age, it can be found that the dosage of NA has obvious impact on ICR: the addition of NA enhances ICR, and this improvement is strengthened with the increase of dosage. In comparison with the reference sample, 4.0% NA heightens ICR by 7% at 28 d, 20% at 90 d, and 29% at 180 d. Furthermore, ICR value is altered with the increase in curing age. In reference sample, ICR is reduced by 11% from 28 d to 90 d and by 19% from 28 d to 180 d. In CAN0.25-CNA2, the same tendency is also observed, but in CNA4, surprisingly, the opposite is true. This result indicates that NA can improve the ICR at the long age.

ICR is related to chemical reaction, physical adsorption, and migration resistance, and more details are presented in the following text.

3.2. Chemical binding

The amount of chloroaluminates in hydrates is closely related to chemical binding, and these hydrates were characterized by TGA, XRD and ^{27}Al NMR.

As presented in Fig. 3, decomposition peaks of FS, KS and CH are marked in the DTG patterns [36–40]. In Fig. 3a, at the age of 28 d,

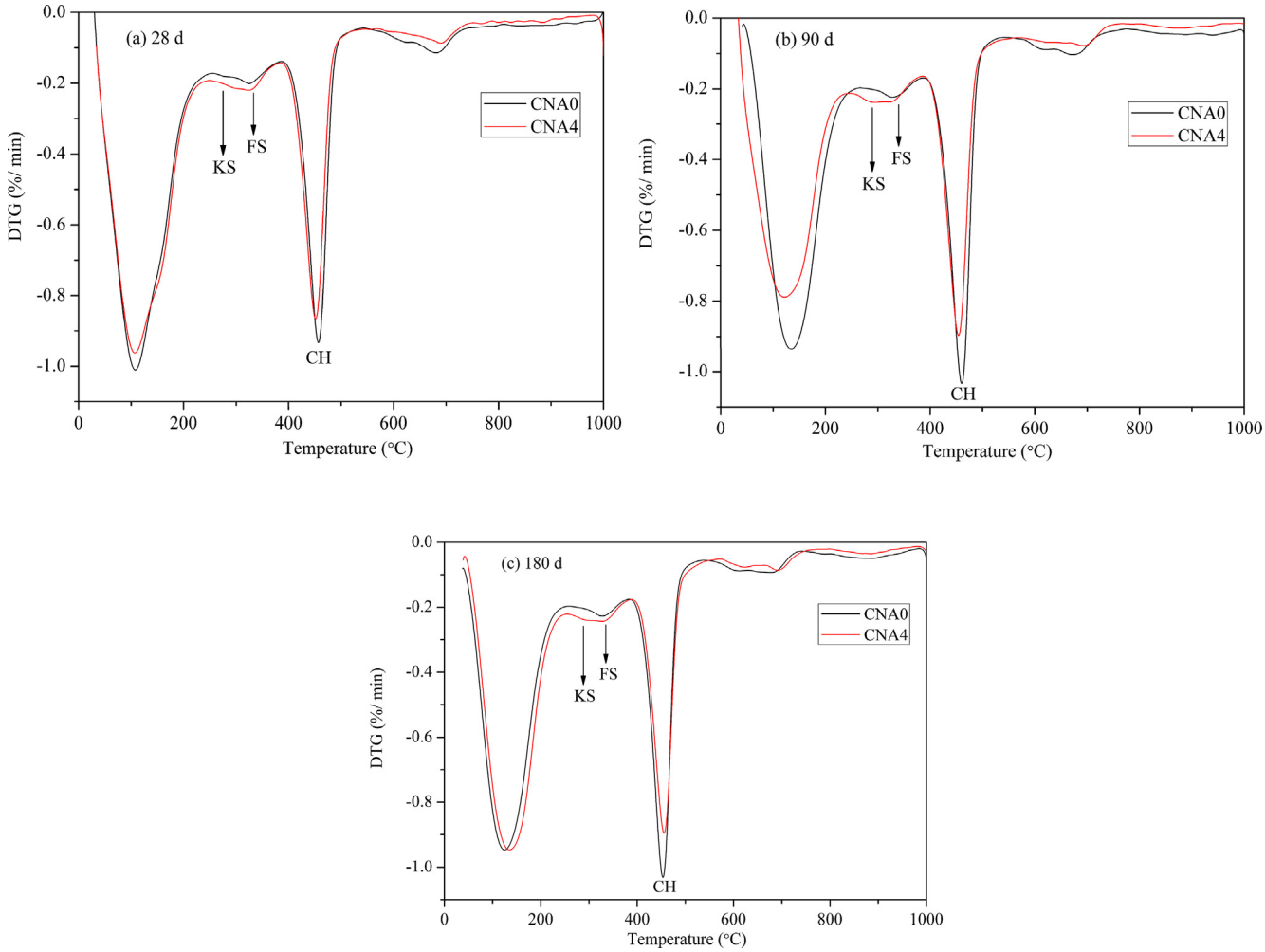

Fig. 3. DTG patterns of CNA0 and CNA4 hydrated for (a) 28 d, (b) 90 d, and (c) 180 d (FS: Friedel's salt, KS: Kuzel's salt, CH: calcium hydroxide).

peaks of FS and KS in CNA4 are higher than those in CNA0; and in Fig. 3b and c, when the curing age extended to the ages of 90 d and 180 d, intensities of peaks of chloroaluminates, especially KS, are significantly increased by the addition of NA.

Fig. 4 presents the XRD patterns of CNA0 and CNA4 hydrated for different ages. In Fig. 4a, at the age of 28 d, the peaks of FS (ICSD #62363) and KS in CNA4 are respectively higher than those in CNA0 [23,41]. And these gaps of peak intensities become more obvious when the curing age extends to 90 d and 180 d in Fig. 4b and c. These results indicate that the addition of NA increases the contents of chloroaluminates by participating the pozzolanic reaction and dissolving aluminum ions into solution.

In addition, the extension of the curing age also affects the phase equilibrium. From 28 d to 90 d, the peak intensity of FS is significantly reduced, while that of KS increases. Based on the fact that FS and KS with the high similarity in molecular structures are produced by the binding of AFm structure $[[Ca_2Al(OH)_6]_2^+]$ with different ions (Cl^- and SO_4^{2-}), this change may imply a phase transformation from FS to KS. And this transformation occurs at low chloride/sulfate ratio, when FS could not maintain thermodynamic stability [41]. Since FS ($[Ca_2Al(OH)_6{\cdot}2H_2O]_2{\cdot}Cl_2{\cdot}4H_2O$) and KS ($[Ca_2Al(OH)_6{\cdot}2H_2O]_2{\cdot}(SO_4)_{0.5}{\cdot}Cl{\cdot}6H_2O$) have different capacities to bind chloride ions observed from the molecular formula, this phase transformation with the extension of curing age would reduce the chemical binding capacity.

Table 3 shows the contents of FS and KS calculated out through RIR method in Section 2.3.3. And the amount of chloride ion in FS and KS is obtained according to the molecular formulas.

As presented in the table, contents of chloride bound by FS and KS in CNA4 are 0.1243% at 28 d age, 0.1147% at 90 d age, and 0.0878% at 180 d age, and these for CNA0 are 0.1094%, 0.0733%, and 0.0649%. Obviously, the chloride bound by FS and KS in CNA4 at 28 d, 90 d, or 180 d is much more than that of CNA0, indicating that addition of NA enhances the chemical binding.

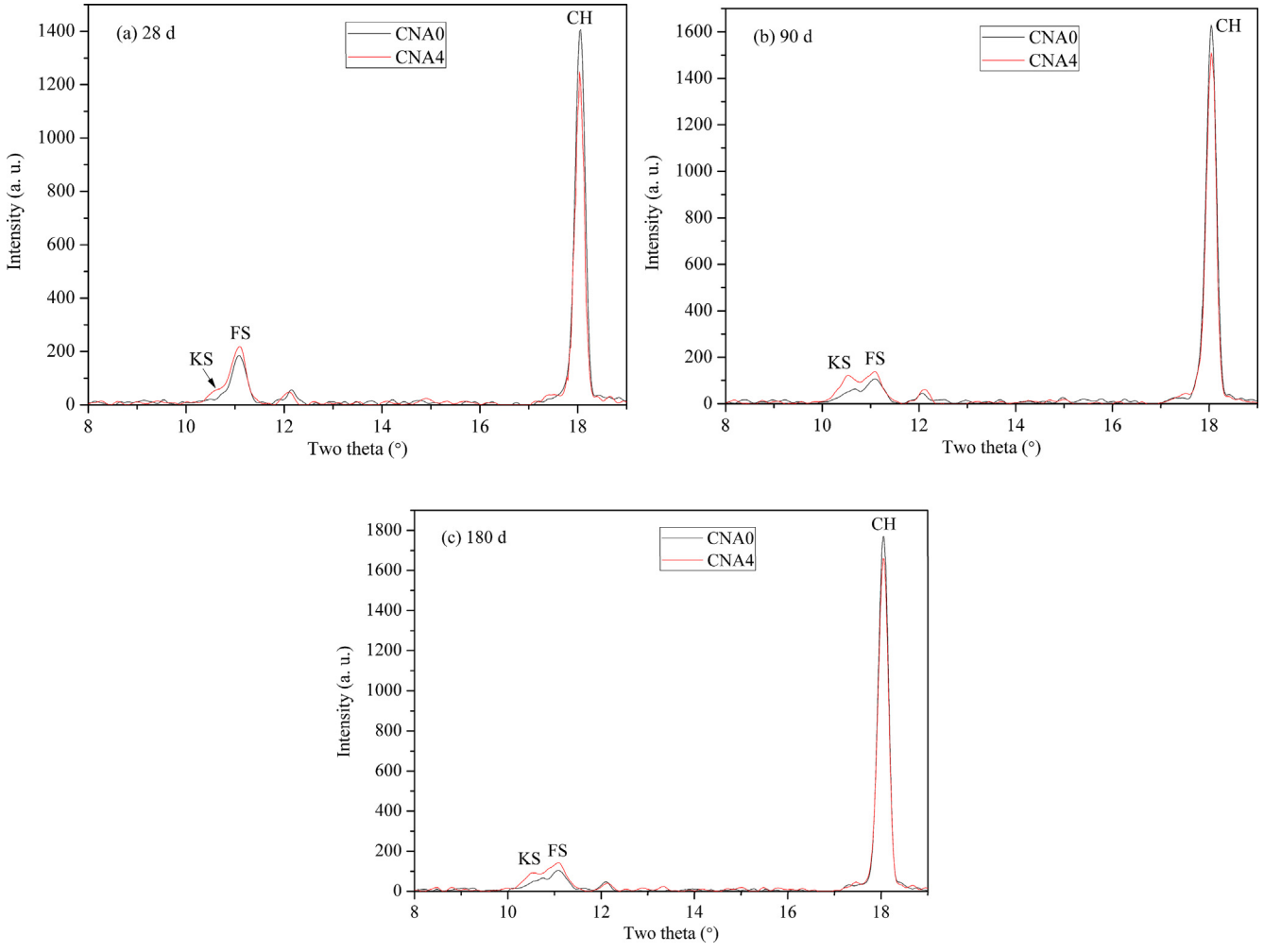

Fig. 4. XRD patterns of CNA0 and CNA4 hydrated for (a) 28 d, (b) 90 d, and (c) 180 d.

Table 3
Contents (wt%) of CH, FS and KS, and contents (wt%) of chloride ions bound by FS and KS.

Sample	CH content	FS content	KS content	Content of chloride in FS and KS
CNA0 at 28 d	20.47	0.82	0.10	0.1094
CNA4 at 28 d	19.11	0.87	0.24	0.1243
CNA0 at 90 d	22.92	0.45	0.29	0.0733
CNA4 at 90 d	20.94	0.64	0.58	0.1147
CNA0 at 180 d	23.11	0.39	0.27	0.0649
CNA4 at 180 d	21.21	0.54	0.35	0.0878

Furthermore, from 28 d to 180 d, the decrease in the value of chemically bound chloride in CNA4 is 29.4%, and that for CNA0 is 40.7%, much higher than that in CNA4. This result demonstrates that addition of NA mitigates the decline in chemical binding capacity at the long age.

To further investigate the effect of NA on the chloroaluminates, ^{27}Al NMR was conducted, and the spectra are showed in Fig. 5. In the spectra, the peak integral intensity depends on the amount of aluminum at the corresponding site. And the octahedral region (Al^{VI}) is ascribed to chloroaluminates at 11.5 ppm and third aluminate hydrates (TAH) at 6.5 ppm [42–44]. According to Andersen et al., TAH represents amorphous calcium aluminate hydrates on particle surfaces of C-S-H grains [45]. And the tetrahedral aluminum (Al^{IV}) near 70 ppm and the penta-coordinated aluminum (Al^{V}) near 35 ppm are related to the aluminum in different sites of the C-S-H gel [46,47].

Fig. 5a presents the distribution of aluminum in the raw material. And the results indicate that peaks of aluminum in NA and cement are respectively near 9 ppm and 80 ppm. The position of these peaks is different from the positions of peaks in Fig. 5b, implying that most of the aluminum in raw materials participates in the hydration reaction and forms new phases at 28 d.

Table 4
Distribution of ^{27}Al sites in different samples.

Sample	Al^{VI} (%)			Al^{V} (%)	Al^{IV} (%)
	chloroaluminates	TAH	Total		
CNA0 at 28 d	44.63	30.77	75.40	3.83	20.77
CNA4 at 28 d	37.82	37.11	74.93	3.27	21.80
CNA0 at 90 d	40.79	38.57	79.36	1.87	18.77
CNA4 at 90 d	33.07	44.75	77.82	1.18	20.99
CNA0 at 180 d	35.30	44.99	80.29	1.71	18.00
CNA4 at 180 d	32.30	44.70	77.00	1.99	21.01

As revealed in Fig. 5b–d, at the same curing age, the peak intensities of chloroaluminates are obviously strengthened by the addition of NA, implying that NA could effectively increase the amount of FS and KS. And Table 4 shows that from 28 d to 180 d, only 5.52% aluminum in chloroaluminates is reduced in CNA4, much less than 9.33% in the reference sample, suggesting the long-term stability of chloroaluminates is significantly improved by adding NA.

Furthermore, Table 4 also reveals that with the extension of the curing age, the amount of aluminum in chloroaluminates is

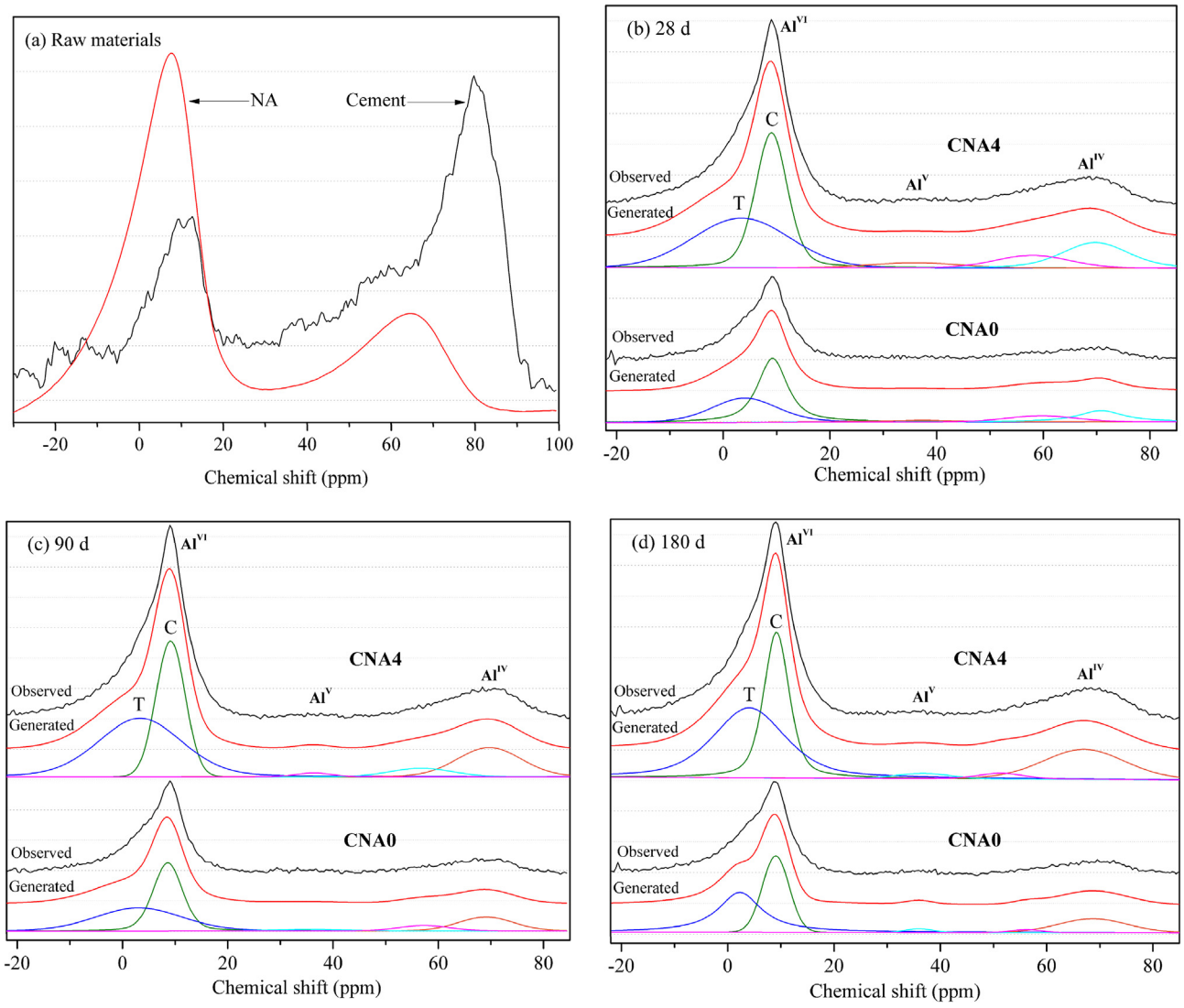

Fig. 5. Deconvoluted ^{27}Al MAS NMR spectra of (a) raw materials, CNA0 and CNA4 hydrated for (b) 28 d, (c) 90 d, and (d) 180 d (C: chloroaluminates, T: TAH). The spectrum of the pure cement in (a) is vertically expanded by 40 times, while the spectra in (b), (c), and (d) are shown on a normalized intensity scale.

reduced, while the opposite is right for TAH. This result suggests that the reduction in the amount of chloroaluminates at the long age is closely related to the formation of TAH.

3.3. Chloride migration resistance

Pore structure is accepted as one of the main factors influencing the chloride migration, and refined pore structure can physically resist the chloride migration by blocking the channel. MIP was conducted to characterize the pore structures of the hardened pastes, and the results are showed in Fig. 6 and Table 5.

Electrical double layer (EDL) was reported to show a strong impact on the migration of chloride ions in the pore diameter less than 10 nm, and the reason was that chloride ion solvated into 2–3 nm cluster could be easily adsorbed by EDL [48–50]; and these structures could further block chloride ions transport in channel, with contribution to chloride migration resistance. Therefore, pore with size less than 10 nm is of great interesting.

As shown in Table 5, the addition of NA increases the volume of pore with size less than 10 nm at the age of 28 d and 180 d, indicating that NA improves the chloride migration resistance. Additionally, with addition of NA, the total porosity and the volume of pore with size greater than 10 nm are reduced regardless of curing age, because of the filling effect of nano particles. These results illustrate the refinement of pore structure by adding NA, with contribution to the chloride migration resistance.

It is noticed that from 28 d to 180 d, NA reduces the volume of pore with size less than 10 nm, and this result illustrates that NA has negative effect on EDL after 28 d age. However, the volume of pore with size larger than 10 nm and the total porosity are significantly reduced in CNA4 with the extension of age, and the refined pores exert positive effect on chloride migration resistance. And this probably shows greater efficacy than that of EDL, thereby higher chloride migration resistance.

3.4. Physical adsorption

3.4.1. Amount of C-S-H gel

Physical adsorption of chloride ions in cement-based materials due to the adsorption of C-S-H gel with electric double layer is mainly decided by amount of C-S-H gel. Therefore, ^{29}Si MAS NMR was adopted to evaluate the amount of C-S-H gel by determine the hydration degree of cement.

The deconvoluted ^{29}Si MAS NMR spectra of samples are plotted in Fig. 7, and the difference between the spectrums of CNA0 and CNA4 can be observed. Peaks named Q^0, Q^1, Q^2 (1Al) and Q^2 are labeled in the figure: Q^0 presents the unhydrated Si-O tetrahedron in cement minerals; Q^1 and Q^2 present the chain end groups and middle-chain groups in the chain of C-S-H gel, respectively; Q^2 (1Al) relates to the middle-chain groups where one of the adjacent tetrahedral sites is occupied by aluminum [51,52]. Based on the fitting and calculation of spectra, three important parameters are obtained in Table 6, including the main chain length (MCL), the Al/Si ratio, and the reaction degree of cement (A_C).

Obviously, at the same age, the Q^0 peak of CNA4 is higher than that of CNA0 in Fig. 7, implying the more amount of unhydrated Si-O tetrahedron in CNA4. And Table 6 reveals that reaction degrees of cement (A_C) of CNA4 are 62.04% at 28 d, 68.15% at 90 d, and 70.62% at 180 d, and these for CNA0 are 66.00%, 70.06%, and 71.37%, which are higher than those in CNA4. These results imply that the addition of NA hinders the hydration of cement and reduces the amount of C-S-H gel.

Furthermore, as suggested in Table 6, the gap of A_C between CNA0 and CNA4 declines with the extension of the age, from 3.96% at 28 d, to 1.91% at 90 d, and further to 0.75% at 180 d, demonstrating that retardation effect of NA on cement hydration is reduced with the age. Consequently, the addition of NA weakens the physical adsorption due to its retardation effect on the formation of C-S-H gel, and this negative effect is decreased with the extension of age.

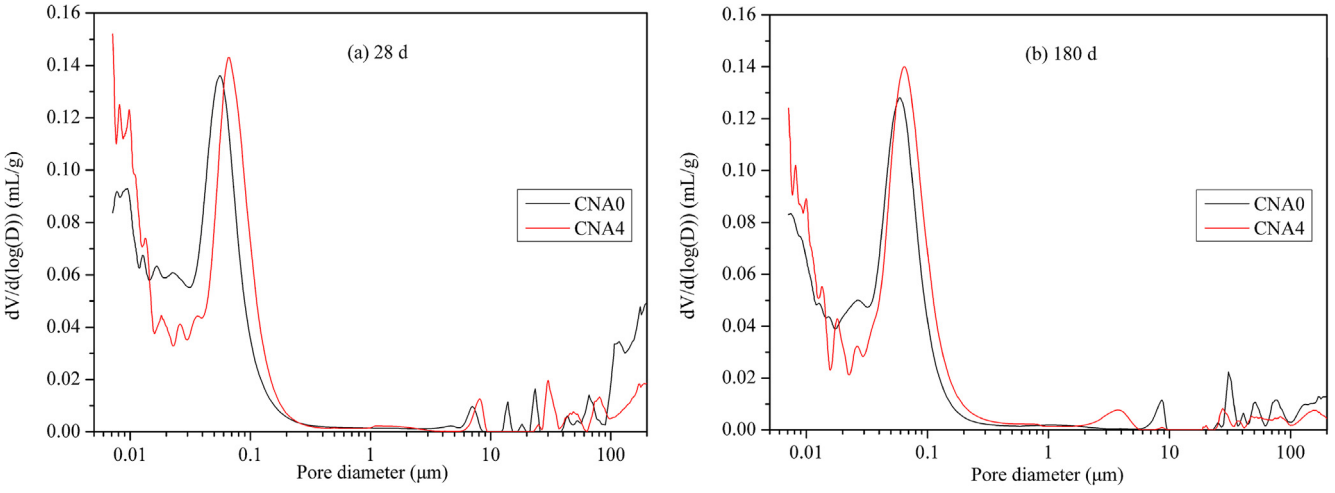

Fig. 6. The pore size distribution of CNA0 and CNA4 at (a) 28 d and (b) 180 d.

Table 5
Pore size distributions of hardened cement-NA pastes at different ages.

Samples	CNA0 at 28 d	CNA4 at 28 d	CNA0 at 180 d	CNA4 at 180 d
Porosity (mL/g)	0.1187	0.1086	0.0988	0.0929
<10 nm pore volume (mL/g)	0.0232	0.0294	0.0208	0.0221
>10 nm pore volume (mL/g)	0.0955	0.0792	0.0780	0.0708

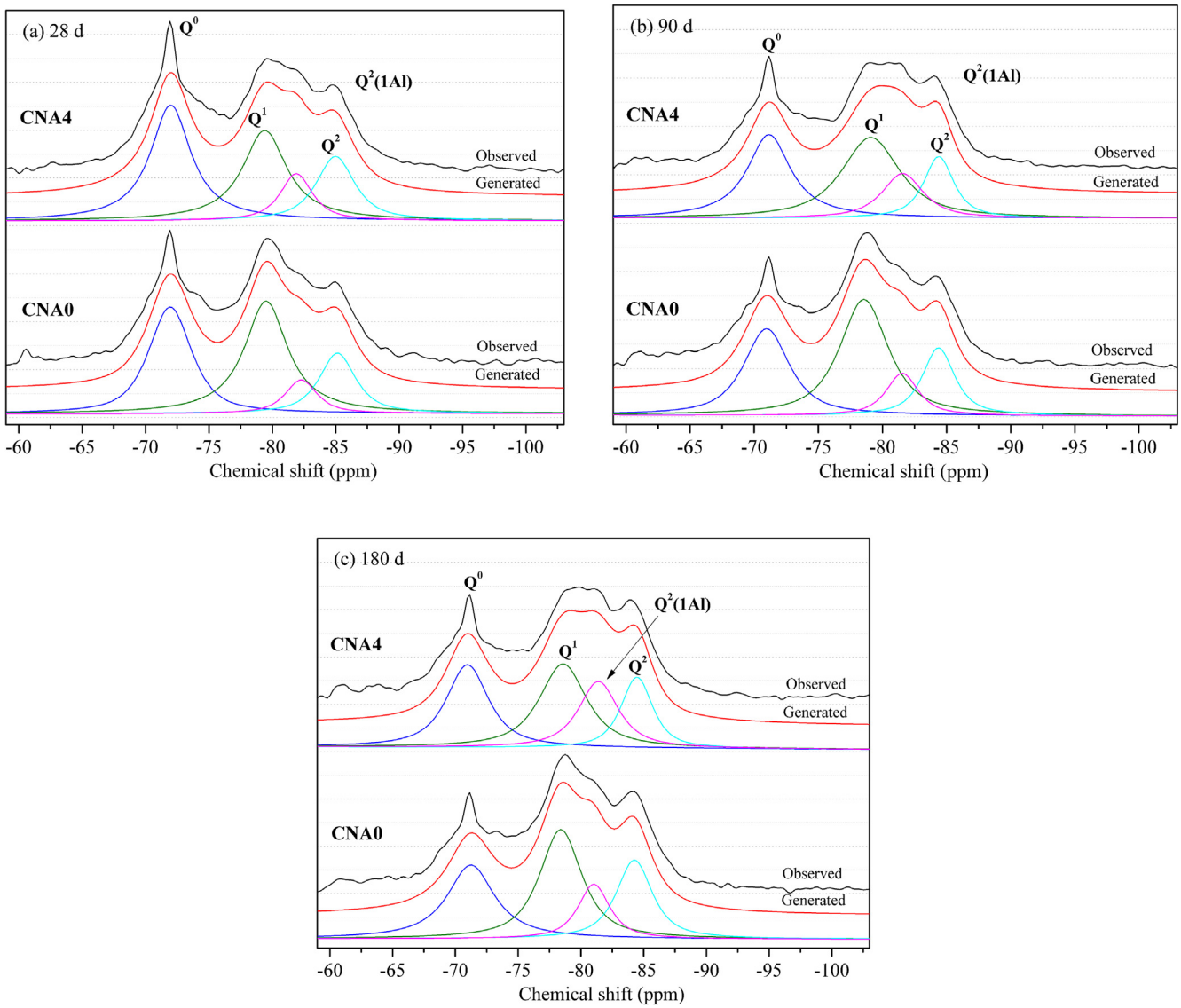

Fig. 7. Deconvoluted ^{29}Si MAS NMR spectra of CNA0 and CNA4 hydrated for (a) 28 d, (b) 90 d, and (c) 180 d. The six spectra are shown on a normalized intensity scale.

Table 6
Deconvolution results of ^{29}Si MAS NMR spectra.

Sample	Q^0 (%)	Q^1 (%)	Q^2 (1Al) (%)	Q^2 (%)	MCL	Al/Si ratio (%)	A_C (%)
CNA0 at 28 d	34.00	40.68	16.96	8.36	3.45	0.06	66
CNA4 at 28 d	37.96	32.36	18.43	11.25	4.18	0.09	62.04
CNA0 at 90 d	29.94	42.94	16.68	10.44	3.51	0.07	70.06
CNA4 at 90 d	31.85	38.24	15.04	14.88	3.95	0.11	68.15
CNA0 at 180 d	28.63	35.87	22.04	13.46	4.35	0.09	71.37
CNA4 at 180 d	29.38	32.95	20.66	17.01	4.8	0.12	70.62

3.4.2. Ca/Si ratio of C-S-H gel

The Ca/Si ratio is reported as another important factor influencing the capacity of C-S-H gel to adsorb chloride ion, and the higher Ca/Si ratio shows stronger capacity [12,16,53]. The average Ca/Si ratio detected by EDS dot scanning is presented in Fig. 8, and the standard deviation is labeled.

Obviously, the Ca/Si ratio in CNA4 is lower than that in the reference sample, regardless of the curing age. This result indicates that the addition of NA decreases the Ca/Si ratio of C-S-H gel. In this case, the physical adsorption is reduced. The reason for the decrease in Ca/Si ratio of C-S-H gel is attributed to the fact that the consumption of CH by the pozzolanic reaction of NA reduces the amount of calcium for the formation of C-S-H gel.

Based on discussion above, it can be found that NA reduced the physical adsorption, and the reason is related to two aspects: the reduced amount of C-S-H gel due to its retardation effect and the decreased Ca/Si ratio by the consumption of calcium.

3.5. Mechanism

The thermodynamic modeling is employed to predict the final phase assemblage for cement-NA system containing NaCl. To make

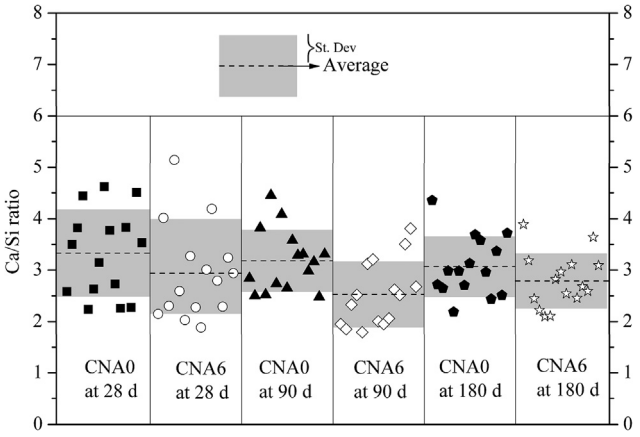

Fig. 8. Ca/Si ratio of C-S-H gel of samples.

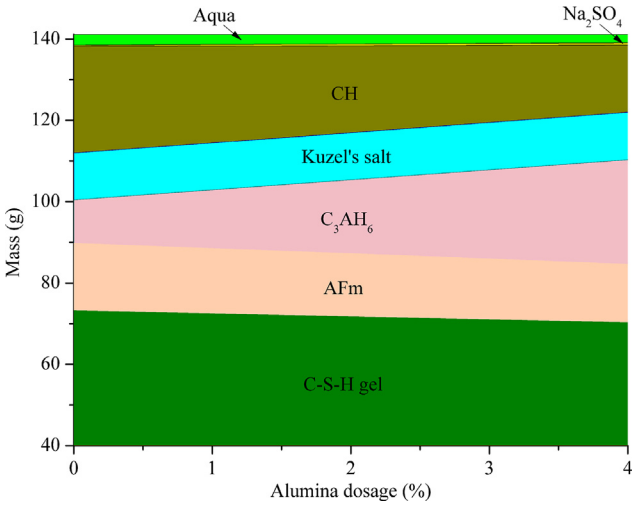

Fig. 9. Phase assemblages for the cement-NA system containing NaCl.

Table 7
The relative volume (vol%) of the capillary pore in hardened pastes at 25 °C, 1 bar.

	CNA0	CNA0.25	CNA0.5	CNA1	CNA2	CNA4
Relative volume	3.11	3.06	3.02	2.95	2.78	2.45

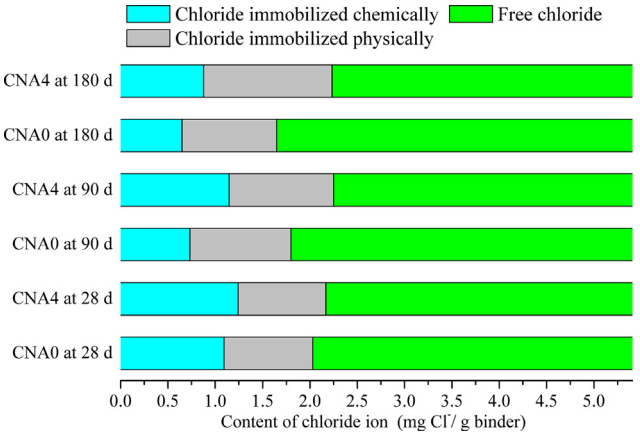

Fig. 10. Schematic description of the chloride distribution in samples.

the prediction easier to understand, this modeling is simplified by assuming the composition of cement as 50% C_3S, 25% C_2S, 20% C_3A and 5% $CaSO_4$. And the results are plotted in Fig. 9.

As revealed in the figure, the final phase assemblage of the cement-NA system contained C-S-H gel, CH, AFm, KS, C_3AH_6, Na_2SO_4, and with the increase of NA dosage, CH decreases and C_3AH_6 increases. The main difference in phase assemblage between the measurement and the prediction is the tested FS and TAH, and the predicted AFm and C_3AH_6. It results from the fact that the hydration at the age of 180 d still could not reach the final equilibrium. Under this thermodynamic imbalance state, the transformation from FS to KS is observed in XRD, probably accompanied with the formation of slight amount of AFm [23,41,54]. Therefore, the thermodynamic modeling illustrates the instability of FS, and predicts the future phase assemblage.

Moreover, the thermodynamic model also predicts the relative volume of the capillary pore as revealed in Table 7, based on the fact that the space occupied by the unreacted water in the cement paste would eventually be converted into the space of capillary pores. It implies that the volume of the capillary pore is reduced by adding NA, promoting the resistance to chloride migration.

As plotted in Fig. 10, the chloride inside the cement-based materials could be quantitatively divided into three parts: a) the content of free chloride ion, directly determined by the titration; b) the chemically immobilized chloride ion, related to the chloride in FS and KS presented in Table 3; c) the physically immobilized chloride, ascribed to the physical adsorption by C-S-H gel and the migration resistance.

Evidently, CNA4 immobilizes more chloride ion than the reference sample, irrespective of the curing age. The addition of 4% NA increases the amount of chemically immobilized chloride, resulting from the fact that NA facilitates the formation of chloroaluminates and increases their stability at the long age. The reasons for the increase in physically immobilized chloride by adding NA could be ascribed to the fact that the positive effect of refinement byNA on migration resistance is stronger than the negative effect on the adsorption of C-S-H gel. And with the extension of the curing age, the retardation effect on producing C-S-H gel is declined, resulting in the further increase of physically immobilized chloride.

4. Conclusions

The addition of NA has a great influence on the chloride immobilization. In control sample, ICR of cement decreases with age; after the addition of NA, the situation improves significantly, and sample added with 4% NA could even obtain the higher ICR at the age of 180 d.

Based on the measurement results, the mechanism of NA changing ICR could be revealed from three aspects: a) chemical binding is strengthened by increasing the content of chloroaluminates formation; b) the migration resistance is enhanced by refining the pore structure; c) physical adsorption is decreased negligibly, due to the fact that the addition of NA slightly reduced the amount and Ca/Si ratio of C-S-H gel.

The final results of these three parts are the effective enhancement of ICR at the age of 90 d and 180 d. It provides a promising way to improve the long-term chloride immobilization capacity. Therefore, the application of NA in chloride immobilization is expected to provide guidance for the development of marine resources

Declaration of Competing Interest

None.

Acknowledgement

The financial support from National key R&D program of China (2016YFC0701003-5) is gratefully acknowledged.

References

[1] C. Monticelli, A. Frignani, G. Trabanelli, A study on corrosion inhibitors for concrete application, Cem. Concr. Res. 30 (4) (2000) 635–642.
[2] W. Morris, M. Vázquez, A migrating corrosion inhibitor evaluated in concrete containing various contents of admixed chlorides, Cem. Concr. Res. 32 (2) (2002) 259–267.
[3] A. Chenan, S. Ramya, R.P. George, Mudali U. Kamachi, Hollow mesoporous zirconia nanocontainers for storing and controlled releasing of corrosion inhibitors, Ceram. Int. 40 (7) (2014) 10457–10463.
[4] B. Martin-Perez, H. Zibara, R.D. Hooton, M.D.A. Thomas, A study of the effect of chloride binding on service life predictions, Cem. Concr. Res. 30 (8) (2000) 1215–1223.
[5] B.G. Ma, T. Zhang, H.B. Tan, X.H. Liu, J.P. Mei, W.B. Jiang, et al., Effect of TIPA on chloride immobilization in cement-fly ash paste, Adv. Mater. Sci. Eng. (2018).
[6] R. Loser, B. Lothenbach, A. Leemann, M. Tuchschmid, Chloride resistance of concrete and its binding capacity – Comparison between experimental results and thermodynamic modeling, Cem. Concr. Compos. 32 (1) (2010) 34–42.
[7] Z.Y. Qu, Q.L. Yu, H.J.H. Brouwers, Relationship between the particle size and dosage of LDHs and concrete resistance against chloride ingress, Cem. Concr. Res. 105 (2018) 81–90.
[8] A. Delagrave, J. Marchand, J.P. Ollivier, S. Julien, K. Hazrati, Chloride binding capacity of various hydrated cement paste systems, Adv. Cem. Based Mater. 6 (1) (1997) 28–35.
[9] T. Pan, K. Xia, L. Wang, Chloride binding to calcium silicate hydrates (C-S-H) in cement paste: a molecular dynamics analysis, Int. J. Pavement Eng. 11 (5) (2010) 367–379.
[10] B. Zhang, H. Tan, W. Shen, G. Xu, B. Ma, X. Ji, Nano-silica and silica fume modified cement mortar used as Surface Protection Material to enhance the impermeability, Cem. Concr. Compos. 92 (2018) 7–17.
[11] R. Luo, Y.B. Cai, C.Y. Wang, X.M. Huang, Study of chloride binding and diffusion in GGBS concrete, Cem. Concr. Res. 33 (1) (2003) 1–7.
[12] A. Dousti, M. Shekarchi, R. Alizadeh, A. Taheri-Motlagh, Binding of externally supplied chlorides in micro silica concrete under field exposure conditions, Cem. Concr. Compos. 33 (10) (2011) 1071–1079.
[13] A. Dousti, J.J. Beaudoin, M. Shekarchi, Chloride binding in hydrated MK, SF and natural zeolite-lime mixtures, Constr. Build. Mater. 154 (2017) 1035–1047.
[14] Z. Shi, M.R. Geiker, K. De Weerdt, T.A. Østnor, B. Lothenbach, F. Winnefeld, et al., Role of calcium on chloride binding in hydrated Portland cement–metakaolin–limestone blends, Cem. Concr. Res. 95 (2017) 205–216.
[15] Z. Shi, Z. Shui, Q. Li, H. Geng, Combined effect of metakaolin and sea water on performance and microstructures of concrete, Constr. Build. Mater. 74 (2015) 57–64.
[16] H. Zibara, R.D. Hooton, M.D.A. Thomas, K. Stanish, Influence of the C/S and C/A ratios of hydration products on the chloride ion binding capacity of lime-SF and lime-MK mixtures, Cem. Concr. Res. 38 (3) (2008) 422–426.
[17] M.V.A. Florea, H.J.H. Brouwers, Chloride binding related to hydration products Part I: ordinary Portland Cement, Cem. Concr. Res. 42 (2) (2012) 282–290.
[18] B.G. Ma, X.H. Liu, H.B. Tan, T. Zhang, J.P. Mei, H.H. Qi, et al., Utilization of pretreated fly ash to enhance the chloride binding capacity of cement-based material, Constr. Build. Mater. 175 (2018) 726–734.
[19] S. Uthaman, V. Vishwakarma, R.P. George, D. Ramachandran, K. Kumari, R. Preetha, et al., Enhancement of strength and durability of fly ash concrete in seawater environments: synergistic effect of nanoparticles, Constr. Build. Mater. 187 (2018) 448–459.
[20] M. Harilal, V.R. Rathish, B. Anandkumar, R.P. George, M.S.H.S. Mohammed, J. Philip, et al., High performance green concrete (HPGC) with improved strength and chloride ion penetration resistance by synergistic action of fly ash, nanoparticles and corrosion inhibitor, Constr. Build. Mater. 198 (2019) 299–312.
[21] T. Cheewaket, C. Jaturapitakkul, W. Chalee, Long term performance of chloride binding capacity in fly ash concrete in a marine environment, Constr. Build. Mater. 24 (8) (2010) 1352–1357.
[22] C.L. Page, Ø. Vennesland, Pore solution composition and chloride binding capacity of silica-fume cement pastes, Matériaux Et Construction. 16 (1) (1983) 19–25.
[23] M. Balonis, B. Lothenbach, G. Le Saout, F.P. Glasser, Impact of chloride on the mineralogy of hydrated Portland cement systems, Cem. Concr. Res. 40 (7) (2010) 1009–1022.
[24] A. Ipavec, T. Vuk, R. Gabrovšek, V. Kaučič, Chloride binding into hydrated blended cements: The influence of limestone and alkalinity, Cem. Concr. Res. 48 (2013) 74–85.
[25] M.D.A. Thomas, R.D. Hooton, A. Scott, H. Zibara, The effect of supplementary cementitious materials on chloride binding in hardened cement paste, Cem. Concr. Res. 42 (1) (2012) 1–7.
[26] X. Pardal, I. Pochard, A. Nonat, Experimental study of Si-Al substitution in calcium-silicate-hydrate (C-S-H) prepared under equilibrium conditions, Cem. Concr. Res. 39 (8) (2009) 637–643.
[27] G. Land, D. Stephan, Controlling cement hydration with nanoparticles, Cem. Concr. Compos. 57 (2015) 64–67.
[28] Y. Reches, Nanoparticles as concrete additives: Review and perspectives, Constr. Build. Mater. 175 (2018) 483–495.
[29] Z. Yang, Y. Gao, S. Mu, H. Chang, W. Sun, J. Jiang, Improving the chloride binding capacity of cement paste by adding nano-Al2O3, Constr. Build. Mater. 195 (2019) 415–422.
[30] M. Heikal, M.N. Ismail, N.S. Ibrahim, Physico-mechanical, microstructure characteristics and fire resistance of cement pastes containing Al2O3 nano-particles, Constr. Build. Mater. 91 (2015) 232–242.
[31] B. Ma, T. Zhang, H. Tan, X. Liu, J. Mei, W. Jiang, et al., Effect of TIPA on chloride immobilization in cement-fly ash paste, Adv. Mater. Sci. Eng. 2018 (2018) 11.
[32] J. Geng, D. Easterbrook, Li L-y, Mo L-w. The stability of bound chlorides in cement paste with sulfate attack, Cem. Concr. Res. 68 (2015) 211–222.
[33] H. Tan, X. Zhang, X. He, Y. Guo, X. Deng, Y. Su, et al., Utilization of lithium slag by wet-grinding process to improve the early strength of sulphoaluminate cement paste, J. Cleaner Prod. 205 (2018) 536–551.
[34] M. Liu, H.B. Tan, X.Y. He, Effects of nano-SiO2 on early strength and microstructure of steam-cured high volume fly ash cement system, Constr. Build. Mater. 194 (2019) 350–359.
[35] K. De Weerdt, A. Colombo, L. Coppola, H. Justnes, M.R. Geiker, Impact of the associated cation on chloride binding of Portland cement paste, Cem. Concr. Res. 68 (2015) 196–202.
[36] U.A. Birnin-Yauri, F.P. Glasser, Friedel's salt, Ca2Al(OH)6(Cl, OH)·2H2O: its solid solutions and their role in chloride binding, Cem. Concr. Res. 28 (12) (1998) 1713–1723.
[37] A. Mesbah, M. François, C. Cau-dit-Coumes, F. Frizon, Y. Filinchuk, F. Leroux, et al., Crystal structure of Kuzel's salt 3CaO·Al2O3·1/2CaSO4·1/2CaCl2·11H2O determined by synchrotron powder diffraction, Cem. Concr. Res. 41 (5) (2011) 504–509.
[38] R.O. Grishchenko, A.L. Emelina, P.Y. Makarov, Thermodynamic properties and thermal behavior of Friedel's salt, Thermochim Acta 570 (2013) 74–79.
[39] Z.G. Shi, M.R. Geiker, B. Lothenbach, K. De Weerdt, S.F. Garzon, K. Enemark-Rasmussen, et al., Friedel's salt profiles from thermogravimetric analysis and thermodynamic modelling of Portland cement-based mortars exposed to sodium chloride solution, Cem. Concr. Compos. 78 (2017) 73–83.
[40] A. Machner, M. Zajac, M. Ben Haha, K.O. Kjellsen, M.R. Geiker, K. De Weerdt, Chloride-binding capacity of hydrotalcite in cement pastes containing dolomite and metakaolin, Cem. Concr. Res. 107 (2018) 163–181.
[41] A. Mesbah, C. Cau-dit-Coumes, G. Renaudin, F. Frizon, F. Leroux, Uptake of chloride and carbonate ions by calcium monosulfoaluminate hydrate, Cem. Concr. Res. 42 (8) (2012) 1157–1165.
[42] Z. Dai, T.T. Tran, J. Skibsted, Aluminum Incorporation in the C-S-H Phase of White Portland Cement-Metakaolin Blends Studied by Al-27 and Si-29 MAS NMR Spectroscopy, J. Am. Ceram. Soc. 97 (8) (2014) 2662–2671.
[43] Y. Wei, W. Yao, X. Xing, M. Wu, Quantitative evaluation of hydrated cement modified by silica fume using QXRD, Al-27 MAS NMR, TG-DSC and selective dissolution techniques, Constr. Build. Mater. 36 (2012) 925–932.
[44] G.K. Sun, J.F. Young, R.J. Kirkpatrick, The role of Al in C-S-H: NMR, XRD, and compositional results for precipitated samples, Cem. Concr. Res. 36 (1) (2006) 18–29.
[45] M.D. Andersen, H.J. Jakobsen, J. Skibsted, A new aluminium-hydrate species in hydrated Portland cements characterized by Al-27 and Si-29 MAS NMR spectroscopy, Cem. Concr. Res. 36 (1) (2006) 3–17.
[46] M. Saillio, V. Baroghel-Bouny, F. Barberon, Chloride binding in sound and carbonated cementitious materials with various types of binder, Constr. Build. Mater. 68 (2014) 82–91.
[47] G. Paul, E. Boccaleri, L. Buzzi, F. Canonico, D. Gastaldi, Friedel's salt formation in sulfoaluminate cements: A combined XRD and 27Al MAS NMR study, Cem. Concr. Res. 67 (2015) 93–102.
[48] Y. Elakneswaran, T. Nawa, K. Kurumisawa, Zeta potential study of paste blends with slag, Cem. Concr. Compos. 31 (1) (2009) 72–76.
[49] Y. Elakneswaran, T. Nawa, K. Kurumisawa, Electrokinetic potential of hydrated cement in relation to adsorption of chlorides, Cem. Concr. Res. 39 (4) (2009) 340–344.
[50] P. Zhang, D. Hou, Q. Liu, Z. Liu, J. Yu, Water and chloride ions migration in porous cementitious materials: An experimental and molecular dynamics investigation, Cem. Concr. Res. 102 (2017) 161–174.
[51] M.D. Andersen, H.J. Jakobsen, J. Skibsted, Incorporation of aluminum in the calcium silicate hydrate (C-S-H) of hydrated Portland cements: A high-field Al-27 and Si-29 MAS NMR Investigation, Inorg. Chem. 42 (7) (2003) 2280–2287.
[52] B. Ma, T. Zhang, H. Tan, X. Liu, J. Mei, H. Qi, et al., Effect of triisopropanolamine on compressive strength and hydration of cement-fly ash paste, Constr. Build. Mater. 179 (2018) 89–99.
[53] J.J. Beaudoin, V.S. Ramachandran, R.F. Feldman, Interaction of chloride and C-S-H, Cem. Concr. Res. 20 (6) (1990) 875–883.
[54] F.P. Glasser, A. Kindness, S.A. Stronach, Stability and solubility relationships in AFm phases: Part I. Chloride, sulfate and hydroxide, Cem. Concr. Res. 29 (6) (1999) 861–866.